Table II. Extended Hückel Parameters

orbital		H_{ii}, eV	exponent
Te	5s	−20.78	2.51
	5p	−11.04	2.16
Sn	5s	−16.16	2.13
	5p	−8.32	1.82
H	1s	−13.60	1.30

lead to any significant improvement. Interestingly, the reduced overlap populations for atoms that might be involved in this interaction show that indeed there is a small bonding interaction (+0.0039) but there is an antibonding one of similar magnitude (−0.0037) between the darkened Te and the central Te in the Te_5 unit containing the shaded Te. These two interactions are of similar magnitude in all the other geometries. As we move the two trimers toward each other, past the equilibrium separation in the polymer, the Te_p–Te_p' interaction grows more bonding but the above-mentioned Te_p–Te_c' interaction becomes more antibonding. The total energy for the approach of the two trimers is quite repulsive. It appears that our method does not portray properly the origins of what we feel on structural grounds must be a bonding interaction.

In summary, we have examined the electronic structure and bonding in a number of polymers containing the square-planar Te_5 repeating unit. These are seen to be characterized by weaker electron-rich three-center bonds within the unit, which accounts for the elongation of the intraunit Te–Te bond length by ~0.25 Å over a normal bond, and the unit is shown to be an unstable species, compared with, e.g., ICl_4^-. However, the formation of infinite one-dimensional chains due to covalent or dative bonding between units (Te_5^{2-}) or with another modulating atom ($SnTe_5^{2-}$) is energetically sufficient to stabilize the overall structure. In spite of the significant topological difference between the Cs_2Te_5 (cisoid) and Rb_2Te_5 (transoid) chains their electronic structures are virtually identical. These have been interpreted for all three compounds by employing model molecules, which provided a basis for understanding the band structure of the infinite chains. The HOMO in the model compounds is an antibonding orbital within the square-planar unit, leading to the suggestion that modification of the synthesis of these compounds could lead to an oxidized form of the chain with modified properties and greater inherent stability of the Te_5^{n-} units. The electronic basis for the short interchain Te···Te distance of 3.47 Å, reminiscent of a similar contact in elemental tellurium, was investigated but apparently is beyond the capability of the extended Hückel method.

Acknowledgment. J.B. wishes to thank S. Alvarez and J. Silvestre for many helpful discussions. We are grateful to Eleanor R. Stagg for typing the manuscript and to Jane Jorgensen for the figures. Our work was supported by NSF Grant CHE8406119. We have benefited greatly from the comments of a careful and conscientious reviewer. Many of his or her suggestions have been included in the final version of the manuscript.

Appendix

Extended Hückel parameters for all atoms used are presented in Table II. The H_{ii} values are from ref 23, and the exponents are from ref 24.

Registry No. Rb_2Te_5, 88188-94-7; Cs_2Te_5, 83332-22-3; K_2SnTe_5, 86205-22-3; Te, 13494-80-9.

(23) Hinze, J.; Jaffé, H. H. *J. Am. Chem. Soc.* **1962**, *84*, 540–548.
(24) Clementi, E.; Roetti, C. *At. Data. Nucl. Data Tables* **1974**, *14*, 177–478.

Contribution from the Department of Chemistry and Materials Sciences Center, Cornell University, Ithaca, New York 14853

Tetrahedral and Square-Planar One-Dimensional Chains: The Interplay of Crystal Field and Bandwidth in MS_2 Compounds

JÉRÔME SILVESTRE and ROALD HOFFMANN*

Received March 29, 1985

One-dimensional ML_2 chains with edge-sharing tetrahedral or square-planar coordination at the transition metal are the subject of this theoretical analysis. The band structures of these systems are examined in substantial detail. The local ligand field at the metal is a good starting point for an understanding of the band ordering in these extended structures, but inter unit cell interactions, both through the bridges and directly between the metals, are important for setting the energy order and dispersion of the bands and especially for determining unexpected electron counts for semiconducting behavior; one such case is d^6 for the tetrahedral chain. Pairing distortions, chain folding, and uniform contractions and elongations are also studied in some detail for these materials.

The two most frequency encountered geometrical arrangements of four ligands L around a metal atom are tetrahedral (**1**) or square planar (**2**); the complex stoichiometry in both cases in ML_4. If

1

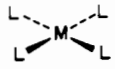

2

the ligand L has the ability to function as a bridge between two metal centers, it is in principle possible to generate from **1** and **2** the polymers **3** and **4**, respectively. The stoichiometry of these

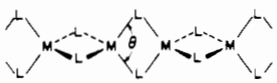

3

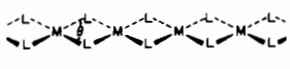

4

chains is $ML_{4/2}$ or ML_2. The magnificent world of structural solid-state chemistry shows us that infinite systems such as **3** and **4** are not just the fruit of our imagination: they do occur in reality.[1]

Table I. Some Known ML_2 Structures

compd	chain	type	θ, deg	M–M, Å	d^n	ref
$KFeS_2$	FeS_2^-	**3**	106.0	2.70	d^5	2a
$RbFeS_2$	FeS_2^-	**3**	105.0	2.71	d^5	2b
$CsFeS_2$	FeS_2^-	**3**	105.0[a]	2.71[a]	d^5	2b, 3
$Na_3Fe_2S_4$	$FeS_2^{1.5-}$	**3**	106.0	2.75	$d^{5.5}$	4
$Na_5Co_2S_5$	$CoS_2^{1.5-}$	**3**	96.0	3.11	$d^{6.5}$	5
Na_2PdS_2	PdS_2^{2-}	**4**	82.5	3.54	d^8	6
Na_2PtS_2	PtS_2^{2-}	**4**	82.5	3.55	d^8	6
K_2PtS_2	PtS_2^{2-}	**4**	81.0	3.59	d^8	7
Rb_2PtS_2	PtS_2^{2-}	**4**	79.1	3.64	d^8	7
α-$PdCl_2$	$PdCl_2$	**4**	87.0	3.34	d^8	8

[a] Average value.

(1) Bronger, W. *Angew. Chem.* **1981**, *93*, 12; *Angew. Chem., Int. Ed. Engl.* **1981**, *20*, 52.

0020-1669/85/1324-4108$01.50/0

In Table I we summarize important structural information relevant to some of the systems known to data that feature a chain of type **3** or **4**. The d-electron count is also indicated; the convention there is to take the alkali-metal atoms as cationic, and each sulfur is counted at 2−. The last assumption presumes no sulfur–sulfur bonding. For the cobalt system in Table I one may rewrite the formula unit as $(Na_5)^{5+}(S)^{2-}(CoS_2)_2^{3-}$, hence affording each cobalt atom in a +2.5 oxidation state. The angle θ is defined in **3** and **4** and may be used as a parameter to describe the atomic arrangements in **3** or **4** for a given M–L bond length. The alternative is to use the metal–metal distance. Not unexpectedly, the edge-sharing tetrahedral topology **3** is found for compounds incorporating Fe or Co, whereas the edge-sharing square-planar geometry **4** occurs for d^8 Pt. Also, it is not surprising to find as a ligand either a halogen or a chalcogen, given the well-established propensity in inorganic chemistry for these atoms to enter 2-fold bridging coordination.

In this paper we investigate the electronic structure of chains of type **3** and **4**. In particular we would like to understand what, if anything, is special about the electron count of the compounds listed in Table I. Are different oxidation states for the metal attainable, and in connection with recent activity in the physics of one-dimensional materials,[9] which properties could one expect? Finally, the electronic structure, stability, and physical properties of **3** and **4** are examined with respect to the geometrical distortion governed by the angle θ. These questions are dealt with on the basis of molecular orbital and band structure calculations carried out at the extended Hückel level. The relevant geometrical and computational details are listed in the Appendix.

The paper is organized as follows: First, the electronic structure of a tetrahedral $(FeS_2)_\infty$ chain is built up from that of the dimer, Fe_2S_6. The bonding and shape of the bands are discussed. Next, we concentrate on the effect of contracting such a chain made of edge-sharing tetrahedra and analyze in some detail the electronic perturbations brought about by opening the angle θ in **3**. Finally, the band structure of chain **4** is constructed by using a fragment approach, and again the influence of θ is discussed. The analysis is used throughout to predict stability and physical properties of hypothetical materials.

Building Up $(FeS_2)_\infty$ and Its Electronic Structure

The chain under construction is illustrated in **5**. Even if all the Fe atoms are chemically equivalent, the unit cell contains two metal atoms and four sulfurs. The smallest translational vector

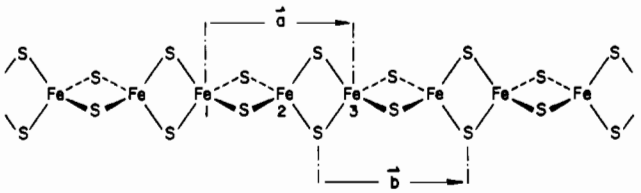

5

that may be used to generate the infinite structure is the vector $\vec{a}$ indicated in **5**, Fe_3 belonging to the next unit cell. Another choice may be vector $\vec{b}$. The four sulfur atoms at the boundaries of the cell thereby defined contribute one-half to the repeat unit. We decided to use this second possibility to construct the electronic structure of **5** because (i) the $Fe_2S_6^{6-}$ dimer[10] (**6**) as well as related

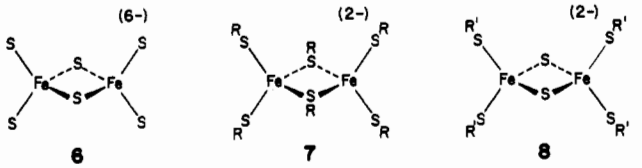

6 **7** **8**

thiolates **7** (R = Et[11]) and **8** (R = *p*-tol[12]) are known, (ii) the orbital pattern of a M_2L_6 system is available from a previous study by Summerville and one of us[13] and therefore only the major features of the analysis need be repeated here, and (iii) the molecular orbitals of **6** will serve as a useful reference when we analyze the topology of the crystal orbitals of **5**.

We now construct the electronic structure of **6**. The details of this process may be found elsewhere,[13] and we shall outline only the details relevant to the present study. With the help of the usual fragmentation approach, the MO interaction diagram for **6** is built-up and displayed in Figure 1.

The geometry at this point is a perfect tetrahedral environment for the two iron atoms, and the Fe–S bond length is 2.26 Å. The resulting Fe–Fe distance is 2.60 Å, the Fe–S–Fe angle is 70.5°, and the overall point group symmetry is D_{2h}. On the left-hand

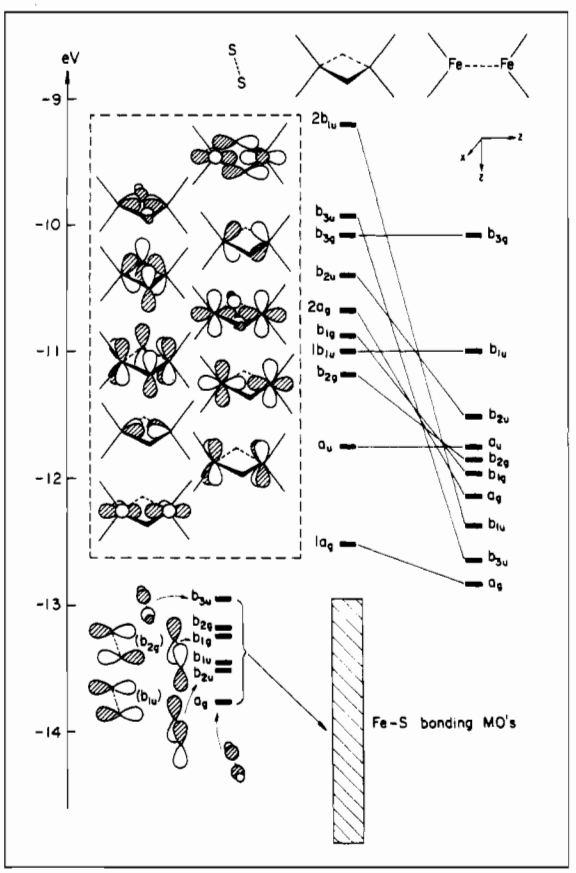

Figure 1. MO diagram for the M_2L_6 frame of **6**. See text.

(2) (a) Boon, J. W.; Mac Gillavry, C. H. *Recl. Trav. Chim. Pays-Bas* **1942**, *61*, 910. (b) Bronger, W. *Z. Anorg. Allg. Chem.* **1968**, *359*, 225.
(3) Bronger, W.; Müller, P. *J. Less-Common Met.* **1980**, *70*, 253.
(4) Klepp, K. O.; Boller, H. *Monatsh. Chem.* **1981**, *112*, 83.
(5) Klepp, K. O.; Bronger, W. *J. Less-Common Met.* **1984**, *98*, 165.
(6) Bronger, W.; Günther, O.; Huster, J.; Spangenberg, M. *J. Less-Common Met.* **1976**, *50*, 49.
(7) Bronger, W.; Günther, O. *J. Less-Common Met.* **1972**, *27*, 73.
(8) Wells, A. F. *Z. Kristallogr., Kristallgeom., Kristallphys., Kristallchem.* **1938**, *100*, 189.
(9) Miller, J. S., Ed. "Extended Linear Chain Compounds"; Plenum Press: New York, 1982; Vol. 1–3. Alcacer, L., Ed. "The Physics and Chemistry of Low-Dimensional Solids"; D. Reidel: Dordrecht, The Netherlands, 1980. Devreese, J. T., Evrard, R. P., Van Doren, V. E., Eds. "Highly Conducting One-Dimensional Solids"; Plenum Press: New York, 1979.
(10) Müller, P.; Bronger, W. *Z. Naturforsch., B.: Anorg. Chem., Org. Chem.* **1979**, *B34*, 1264.
(11) (a) Hagen, K. S.; Holm, R. H. *J. Am. Chem. Soc.* **1982**, *104*, 5496. (b) For different R groups, see also: Henkel, G.; Tremel, W.; Krebs, B. *Angew. Chem.* **1983**, *95*, 317.
(12) Mayerle, J. J.; Denmark, S. E.; DePamphilis, B. V.; Ibers, J. A.; Holm, R. H. *J. Am. Chem. Soc.* **1975**, *97*, 1032. Cleland, W. E., Jr.; Averill, B. A. *Inorg. Chem.* **1984**, *23*, 4192.
(13) Summerville, R. H.; Hoffmann, R. *J. Am. Chem. Soc.* **1976**, *98*, 7240.
(14) Hoffmann, R.; Swenson, J. R.; Wan, C.-C. *J. Am. Chem. Soc.* **1973**, *95*, 7644. Fujimoto, H.; Hoffmann, R. *J. Phys. Chem.* **1974**, *78*, 1167.

side of Figure 1 and lower in energy are the linear combinations of the atomic orbitals centered on the two central sulfur atoms; we find here six combinations, four of which are of pure p type (b_{1u}, b_{2u}, b_{1g}, b_{2g}) whereas some s character mixed in the p_x AO's to produce a_g and b_{3u}.

The right-hand side of Figure 1 presents the ten d-centered orbitals resulting from the combination of two C_{2v} ML_2 fragments. The orbitals of one ML_2 unit have been derived in detail elsewhere.[15] Taking symmetric and antisymmetric combinations (with respect to the xy plane) of two ML_2 fragment orbitals produces the pattern displayed at the right in Figure 1. Allowing the $(ML_2)_2$ and $(S)_2$ fragment orbitals to interact generates the energy level diagram at the center of Figure 1. The orbitals of the S···S unit start low in energy and are pushed down further, providing M–S bonding. Conversely the d orbitals involved in some interactions with the central S_2 unit are shifted up. The resulting molecular orbitals are explicitly drawn out in the dashed-line box for future reference.

The 10 d orbitals emerge rather densely packed in a 3-eV energy range. Although it is difficult to predict within the one-electron theory used in this work the exact magnetic properties of dimers such as **6**, we would believe that for more then four d electrons on each metal the system should be high spin. In particular, for **6** itself with 10 d electrons, the configuration $1a_g^2 1a_u^2 2b_{2g}^1 1b_{1u}^1 1b_{1g}^1 2a_g^1 2b_{2u}^1 1b_{3g}^1$ appears to be the most likely one. This would imply a spin $S = {}^3/_2$ for each Fe, a fact experimentally observed.[1] Similarly, magnetic measurements carried out[16] on a thiophenol derivative of **7** suggest the presence of a high-spin paramagnetic system. A distribution of the 12 electrons such that only $1a_g$ and a_u are doubly occupied would be consistent with the above results. We should however point out that the structure[11] of the molecule under consideration here shows an S–Fe–S angle θ smaller ($\theta = 102.0°$) than the one used in our computations. The corresponding Fe–Fe separation in the structure if 2.98 Å. The fact that the magnetic properties of **6–8** are highly dependent on small geometrical distortions and/or subtle substituent effects is further exemplified by the existence of d^5 low-spin[17] $[Fe_2S_2(S_2\text{-}o\text{-xyl})_2]^{2-}$ and high-spin $Fe_2S_6^{6-}$, even though the Fe_2S_2 cores of both systems are structurally almost equivalent, with a short Fe–Fe distance of 2.70 Å.

Aside from the uncertainties relevant to magnetic properties, we believe that the orbital description of Figure 1 is valid and realistic. We now turn to the electronic structure of the polymeric analogue of **6**, that is **9**. Figure 2 shows the band structure of

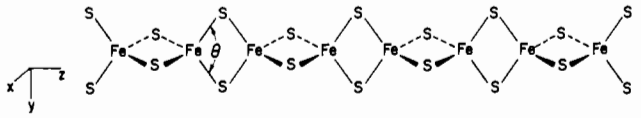

9

9 with $\theta = 109.5°$. The bands are numbered and also labeled according to their symmetry with respect to the xz plane (S or A) and the 4_2 screw axis (+ or −). Notice that most of the bands are folded back at the zone edge ($k = 0.5$, in units of ${}^{2\pi}/_{a}$); this is a direct consequence of the presence of a nonsymmorphic operation, the 4_2 screw axis.[18] The two lines that do not fold represent 2-fold degenerate bands; they are labeled 1E and 2E, with a subscript S or A indicating their symmetry property with respect to the xz plane. Finally, the lowest band within the energy window of Figure 2 is, *at* $k = 0$, centered on the sulfur atoms only and labeled π.

The bands numbered 1–10 are clearly metal d centered and are generated by the 10 d orbitals of Figure 1. The crystal orbitals

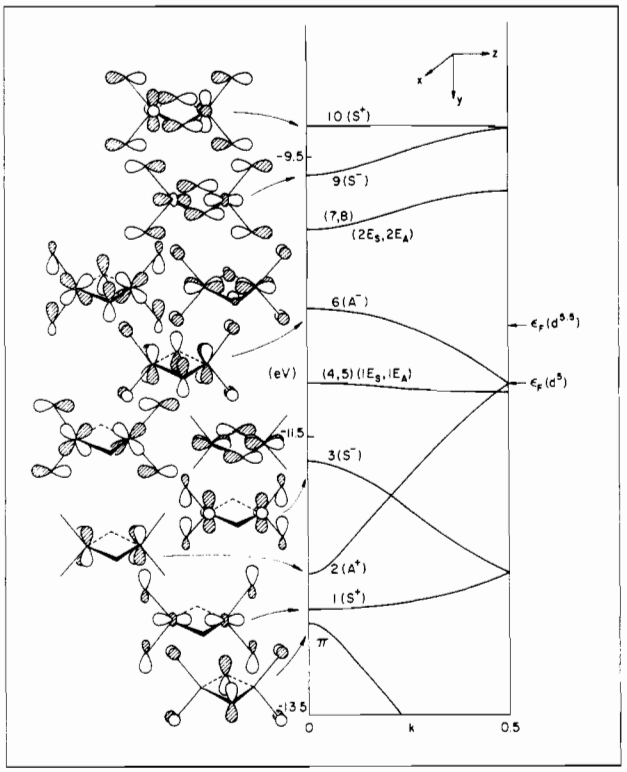

Figure 2. Band structure of the $(FeS_2)_\infty$ chain at $\theta = 109.5°$.

have been drawn out on the left-hand side of Figure 2 with their topology at the zone center, $k = 0$. At this point in the Brillouin zone, the molecular orbitals of the unit cell propagate with a + sign throughout the crystal; in other words the phase of the orbitals on S_5 and S_6 (see **10**) is the same as that on S_1 and S_2, respectively.

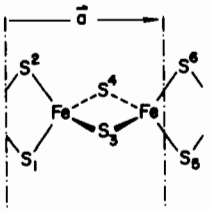

10

The sulfur atoms S_5 and S_6 belong to a unit cell adjacent to that defined by the dashed line in **10**.

The reader will notice that the orbital topology of the bands at $k = 0$ in Figure 2 is not quite the same as that of the orbitals boxed in Figure 1. Also, there are degenerate bands in Figure 2 but no degenerate MO's in Figure 1. All this results from the fact that when one deals with an infinite system such as **9**, the wave functions must be invariant with respect to translational symmetry. In more technical terms, the wave functions at all points of the Brillouin zone must belong to one of the irreducible representations of the group of the wave vector $\vec{k}$, $\tilde{G}_k$. It turns out that at $k = 0$ (and π/a) $\tilde{G}_k$ is (isomorphic with) the full rotational group of the lattice, in our case D_{4h}. Along the line, $\tilde{G}_k$ is isomorphic with the cofactor group of the whole space group with respect to the translational subgroup; here $\tilde{G}_k$ is isomorphic with C_{4v}.[19] Note that the C_{4v} point group contains five irreducible representations and that there are five symmetry labels in Figure 2, S^+, S^-, A^+, A^-, and E. In particular, the C_{4v} group allows the existence of 2-dimensional representations, that is 2-fold degeneracies. In the system under construction, bands no. 4 and 5, their

(15) Albright, T. A.; Burdett, J. K.; Whangbo, M.-H. "Orbital Interactions in Chemistry"; Wiley: New York, 1985. Albright, T. A. *Tetrahedron* **1982**, *38*, 1339.
(16) Tremel, W. Ph.D. Dissertation, University of Münster, 1983.
(17) Holm, R. H.; Ibers, J. A. In "Iron Sulfur Proteins"; edited by W. Lovenberg, W., Ed.; Academic Press: New York, 1977; Vol. 3, p 234.
(18) A nice discussion of the shapes of the bands as a function of the symmetry operations present in the lattice may be found in: Bozovič, J. *Phys. Rev. B: Condens. Matter* **1984**, *29*, 6586.
(19) Excellent presentation of these points may be found in: (a) Burns, G.; Glazer, A. M. "Space Groups for Solid State Scientists"; Academic Press: New York, 1978. (b) Madelung, O. "Introduction to Solid State Theory"; Springer-Verlag: West Berlin, Heidelberg, New York, 1978; Springer Series in Solid-State Sciences, Vol. 2.

k = 0 representatives redrawn in **11** and **12**, are related by one

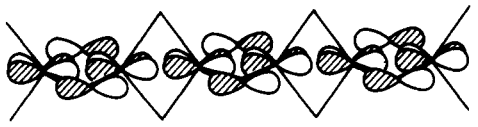

11

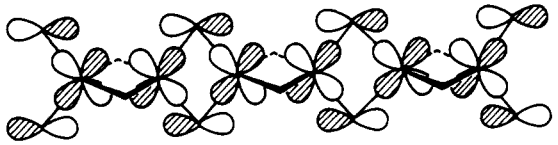

12

of the operations belonging to $\tilde{G}_k$ (4_2) and hence are degenerate. The same argument applies to bands 7 and 8. A further point about these two pairs of degenerate bands is that unlike those bands belonging to one-dimensional representations, they do not fold back at $k = \pi/a$. If this were to occur, one would find at k = π/a a 4-fold degeneracy, which is incompatible with the D_{4h} point group.

The reader will have noticed that band no. 2 is composed purely of metal d character without any sulfur contribution at k = 0. Again, the reason is a symmetry-based one. At the zone center, this band does not find a symmetry-adapted linear combination in D_4h symmetry to mix with. As soon as k departs from 0, the vertical mirror plane is not a symmetry element anymore and $\tilde{G}_k$ becomes C_{4v}, allowing mixing of π and band no. 2. Before the different electron fillings accessible to the system are discussed, we would like to comment on the general topology of the band structure.

First, how are these bands related to the t_2 and e sets we would expect for tetrahedral coordination at one metal? If we refer to Figure 2 and the shape of the crystal orbitals at k = 0, the "t_2" bands are recognizable by σ antibonding between the metal and the sulfurs, found in bands no. 10, 9, 8, 7, 5 and 4. Bands no. 1, 2, 3 and 6 constitute the solid-state analogue of the e set, with π-type overlap between the metal and the sulfur atoms. An interesting point is that one finds a band (no. 6) involved in π bonding *above* the lowest σ-antibonding bands (no. 4,5). This is due to the large π-donating ability of the sulfur ligands, which push the in-phase combination of d_{xy} high in energy. Another reason for this unexpected switch in the level ordering is that the d_{xz} and d_{yz} combinations are pushed up in energy by σ antibonding only to a limited extent in the solid. In a mononuclear tetrahedral complex, these two orbitals would be higher in energy. The difference between the mononuclear and polymeric cases may be understood by using a simple overlap argument. The d_{yz} and d_{xz} orbitals of a ML_4 unit have lobes pointing toward the lone pairs of the ligands (**13a,b**). There is a strong overlap, and large

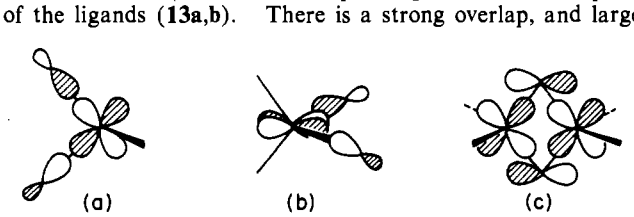

13

destabilization ensues. If one has more than one metal atom, the σ antibonding between bridging atoms and the metals is less, for the lone pairs cannot by symmery be as directional as in the mononuclear case. In **13c** we represent one d component involved in σ antibonding with bridging atoms in a binuclear complex; the overlap in the latter is more "tangential" in nature, rather than "radial" as in **13a** (or **13b**). Note than that this positioning of a π type of orbital above some σ ones should also occur for the binuclear system; in Figure 1, b_{1g} does lie above b_{2g}.

Looking back at Figure 2, one notices that the metal d character in bands 9 and 10 is different; the latter contains mainly $d_{x^2-y^2}$, and the former contains d_{z^2}. The same considerations apply to bands 1 and 3. What is at work here is an avoided crossing between band 9 and band 3, both of S^- symmetry. Technically, band 10 should touch at k = 0 with band 3 whereas band 9 should meet band 1 at this point of the zone. The crucial consequence of this avoided crossing is the creation of a band gap between band 6 and bands 7 and 8. This gap is 0.4-eV wide at k = 0, and 1.4-eV wide at $k = \pi/a$. We would predict therefore that for a 12-d-electron system, in other words *for a d^6Fe atom, the corresponding material should be a semiconductor.* Of course, this assumes a low-spin d^6 iron. The justification for this lies perhaps in the fact that the d^5 $CsFeS_2$ system is low spin with $S = {}^1/_2$ at each metal center.[1] Recall also that the d^6 dimer $Fe_2S_2(S_2\text{-}o\text{-xyl})^{2-}$ is also a low-spin complex.[17]

Most of the materials synthesized to date feature the iron atom in a d^5 electronic configuration. The corresponding Fermi level is indicated with an arrow in Figure 2, at the junction point between bands 2 and 6, at $k = \pi/a$. We encounter here the typical situation leading to a first-order Peierls distortion.[20] A band gap should open between bands 2 and 6, at $k = \pi/a$. The simplest structural deformation allowing this process to occur is the pairing distortion shown in **14a,b**. This can be achieved by an alteration

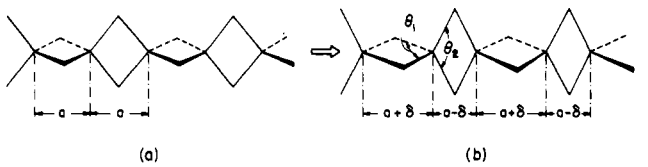

14

in the metal–metal separation, which may also be described by the angular distortion $\theta_2 > 109.5° > \theta_1$ see **14b**. Figure 3 shows at the right the band structure in the vicinity of the Fermi level provided by our computations with θ_1 = 108.0° and θ_2 = 111.0°. At left is the band structure obtained for $\theta_1 = \theta_2$ = 109.5°, extracted from Figure 2. Several points may be made concerning Figure 3b.

Due to the distortion, the symmetry of the system is lowered; in particular $\tilde{G}_k$ is now isomorphic with C_{2v}. Therefore the bands in Figure 3b have been labeled according to their symmetry property with respect to the xz and yz planes. Another consequence of the reduced symmetry is the splitting of the previously degenerate bands 4, 5 and 7, 8.

As anticipated, the degeneracy of bands 2 and 6 at the zone edge is lost. However the magnitude of the gap introduced is very small, E_g = 0.032 eV for $\theta_2 - \theta_1$ = 3.0°. The reason is that the avoided crossing, which is the key to the gap, is very weak. It does take place though; look at the phase relationship between the d orbitals of Fe_1 and Fe_2 at $k = \pi/a$ in band 2 and 6—the two orbitals are out-of-phase in the former and in-phase for the latter. This is the opposite at k = 0. In order to understand better the factors governing the size of the gap, let us focus on the two bands 6 and 2 at k = 0.5. These are redrawn in **15a** and **15b**,

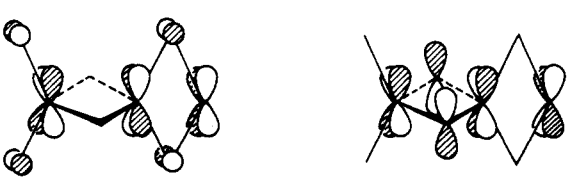

15

(20) Peierls, R. E. "Quantum Theory of Solids"; Oxford University Press: London, 1955; p 108.

respectively. Suppose one increases the distortion; in other words one increases the difference in $\theta_2 - \theta_1$ in **14b**. **15** should be pushed up in energy since the sulfur–metal interactions become more and more antibonding. Conversely, **15b** should be shifted down because the metal–sulfur (antibonding) interactions would be decreased. This follows from a decrease in the overlap between the sulfur p orbitals and the metal d orbitals, as illustrated from a top view in **16**. Therefore, on the basis of the metal–sulfur interaction

16

only, the gap should become larger. However, our computations show that this is not so. The size of the gap actually diminishes upon increasing distortion. The reasons for this lie in the metal–metal and sulfur–sulfur interactions. In **15a**, upon opening of θ_2, the metal–metal interaction becomes more and more bonding and overrides the destabilizing effect of the more antibonding metal–sulfur interactions. Conversely, in **15b**, closing θ_1 increases the repulsion between the two sulfur p orbitals and counterbalances the favorable effect of the diminished metal–sulfur antibonding discussed above.

Eventually, further distortion reopens the gap. This is clearly seen in a Walsh diagram for bands 6 and 2 at $k = \pi/a$, schematically depicted in **17**. The band gap is reopened if the chain

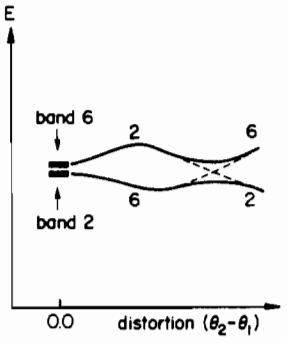

17

is further contracted, due to the reversal of the initial avoided crossing. This is indicated with a dashed line. Overall what this means is that if a Peierls distortion is likely in the d^5 systems, the accompanying structural distortion may be extremely small. In fact, of all the d^5 systems structurally characterized, only in one instance was a slight bond alteration detected (C_5FeS_2[2b,3]). Recall also that this system was reported to be low spin.

Returning to Figure 3b, the reader will have noticed that the top of band 5 lies above the bottom of band 6. It follows that, due to the so-called Wilson transition,[21] schematically depicted in **18**, *if all the lowest states are doubly occupied*, the system should be metallic. However, the relative flatness of bands 4–6 leads us to think that on-site electronic repulsions rule out the possibility of double occupancy of all the lowest electronic states.[22] We believe that, in a block representation, the electronic structure of the distorted chain could be that shown in **19**, with 2 bands

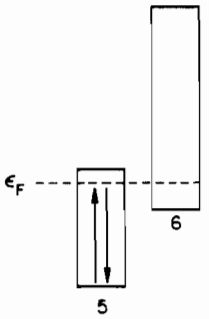

18

being filled with unpaired spins. The dashed line marked ϵ_F in

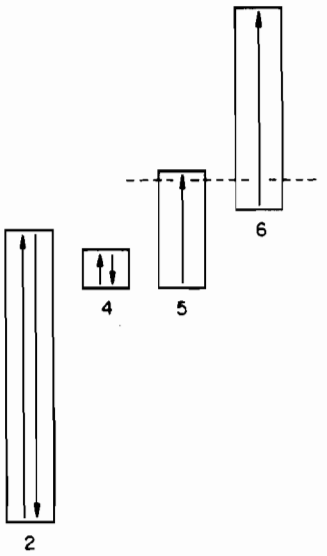

19

19 stands for the Fermi level in the hypothetical case of double occupancy of the lowest energy levels.

It is clearly difficult to predict the exact electronic configuration of the $(FeS_2)_\infty$ chain from the one-electron theory used in this work. However, the flatness of the bands around ϵ_F is defined sufficiently well so that the observed magnetic properties of the system may be accounted for. Finally, it should be pointed out that from the picture of **19** one would predict a magnetic moment corresponding to one unpaired electron per metal ion; this view is supported by the experimental information available.[1]

As indicated in Table I, a system is known with 11 d electrons. If we return to Figure 2, the corresponding Fermi level is indicated by $\epsilon_F(d^{5.5})$. Band 6 is half-filled if the spins are paired, or to put it in a different way, the whole band generated by the d_{xy} orbital on each metal is three-fourths-filled. From this point of view two structural distortions can occur: dimerization or tetramerization. The features relevant to the two cases may be found in Whangbo's papers,[22a,b,d] and we refer the reader to these for detailed explanations. For our purpose it is sufficient to explore here the consequences of the two possibilities offered. In **20a** is given the picture resulting from tetramerization, a $2k_f$ distortion. All electrons are paired up and found in the lowest three of four subbands arising from quadrupling the contents of the unit cell. On the left, in **20b**, is the picture corresponding to a $4k_F$ distortion. Here only two subbands arise, since dimerization simply doubles the unit cell. The lowest subband is fully occupied with paired spins whereas the upper one is fully occupied also, but with unpaired spins. It should be clear from the earlier discussion that the $4k_F$ distortion will be favored; again the reason is that the upper portion of the d_{xy} band (or band 6 in Figure 2) is relatively flat, and therefore only a very small gap could be opened between the third and the fourth band in **20a**. If we assume then that band

(21) See: Reference 19b; pp 363–364.
(22) (a) Whangbo, M.-H. *J. Chem. Phys.* **1979**, *70*, 4963; *Inorg. Chem.* **1980**, *19*, 1729. (b) Whangbo, M.-H.; Foshee, M. J.; Hoffmann, R. *Inorg. Chem.* **1980**, *19*, 1723. (c) Whangbo, M.-H. In "Crystal Chemistry and Properties of Materials with Quasi-One-Dimensional Structures"; Rouxel, J., Ed.; D. Reidel: Dordrecht, The Netherlands, 1985. (d) Whangbo, M.-H. *Acc. Chem. Res.* **1983**, *16*, 95.

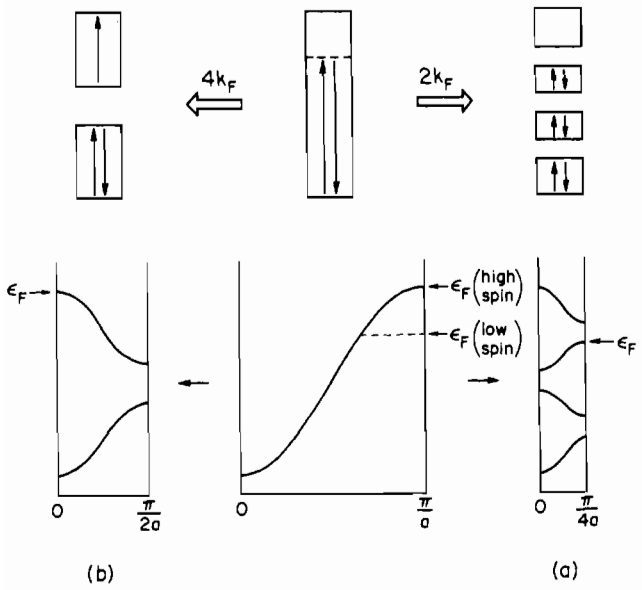

20

6 in Figure 3 would be 100% occupied with unpaired spins, the system would show a tendency to dimerize as **14b**.

The $d^{5.5}$ material reported, however, distorts further. The structure is drawn out in a somewhat idealized manner in **21**. The

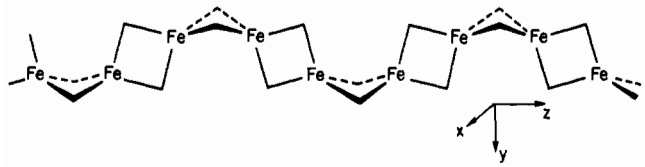

21

metal atoms retain approximate tetrahedral coordination but the metal–metal spine is not linear anymore and rather resembles that of the carbon backbone in *trans*-polyacetylene. It is furthermore important to notice that the unit cell contains four Fe atoms and that all the metal–metal distances are equal within experimental error. Finally, the real structure possesses only a glide plane (xz) as an element of symmetry, whereas our picture in **21** includes also a mirror plane (yz).

In the following we examine the possible reasons for the structure to distort from **14b** to **21**. A good starting point is to realize that, unlike in the high-spin d^5 system, the *top* of band 6 is filled. The major characteristics of the crystal orbitals of this band near the zone center are strong metal–sulfur π-antibonding interactions; these are actually responsible for pushing the in-phase combination of the xy orbitals above its out-of-phase counterpart (band 2 at $k = 0$).

We believe that the system in its desire to diminish these unfavorable interactions may distort in such a way as to hybridize one set of sulfur orbitals away from the metal. Just as in discrete molecules, one way to accomplish this is a distortion allowing the mixing of a higher lying empty band, that is a second-order Jahn–Teller distortion.[23] The candidate of choice for this task is band 7 in Figure 3, and the deformation is that destroying the xz mirror plane. The resulting structure looks like **22**. A calculation of **22** with $\alpha = 10.0°$ and with the metal–metal distances kept equal shows band 6 to be indeed stabilized, although not by much, <0.1 eV. Note that the unit cell in **22** is relatively complex due to the existence of a 2_1 screw axis, which folds back the bands shown in Figure 3. In **23** is depicted the topology of band 6 at

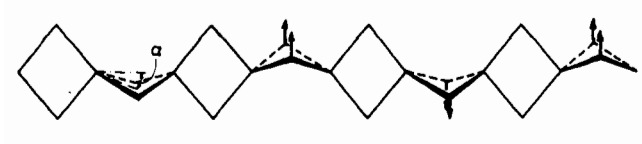

22

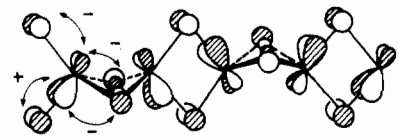

23

$k = 0$ after the distortion **22**. As anticipated, some metal xz has mixed in xy to tilt the resulting orbital. More importantly, out of the initial four metal–sulfur π-antibonding interactions, three have been decreased in intensity, indicated by a minus sign in **23**, while one turns out to be slightly reinforced (+).

The system apparently looks for further stabilization when it undergoes the "buckling" motion, which distorts **22** into the observed geometry **21**. The last unfavorable metal–sulfur interaction is decreased, and our calculation on a reasonable geometry for **21** points to a further stabilization of **23** by ~0.1 eV. However, the driving force for this motion may lie elsewhere. In particular we find that the top of band 2 in Figure 3 is substantially pushed down in energy in the process. A careful look at the composition of the crystal orbital shows that some metal–metal-bonding interaction may be turned on. Note that this would tend to oppose the bond alteration initially required by the $4k_F$ distortion. This would also account for similar metal–metal distances along the chain as reported by Klepp and Boller.[4] We believe, however, that the closeness of the distances in the structure is accidental. The equality of the metal–metal distances is not in fact a symmetry requirements of the structure.

Perhaps a word of caution must be added here. When subtle distortions in solid-state structural chemistry are dealt with, one must be aware of the fact that crystal packing forces and Madelung energy factors can override electronic preferences. In particular for the $d^{5.5}$ compound the stoichiometry is $Na_3Fe_2S_4$ and not $AFeS_2$ (A = Na, K, Cs), as in all the d^5 systems. This means that the structure must accomodate half of an alkali-metal atom more per FeS_2 formula unit. In the above discussion we offer electronic arguments that could justify the observed distortion in $Na_3Fe_2S_4$. It is however difficult for us to tell whether these electronic factors actually drive the deformation.

From the band structure of **21** we would predict band 6 to be fully occupied with unpaired spins. The fact that band 6 is the highest occupied one is supported by the experimentally observed increase in the Fe–S bond lengths in the $d^{5.5}$ system compared to those in the d^5 structures. As noted earlier this band is metal–sulfur antibonding. We would predict $Na_3Fe_2S_4$ to exhibit magnetic behavior and await experimental results to support this suggestion.

Uniform Contraction of the Chain: Electronic Consequences

The electronic and optical properties of a discrete transition-metal complex are largely determined by the crystal field splitting of the metal d orbitals, that is basically the strength of the metal to ligand interaction. In turn, the latter depends on the molecular symmetry, which dictates the amount of overlap between a metal orbital and an appropriate combination of ligand atomic functions.[24] If one brings 10^{23} such units together to form an extended structure, the physical properties of the system are now governed by crystal field effects—site symmetry factors—and band dispersion–interunit interactions. In the following we examine the relative importance of these effects in a $(MS_2)_\infty$ edge-sharing tetrahedral chain as a function of a uniform deformation—contraction or elongation—of the lattice.

(23) Öpik, U.; Pryce, M. H. L.; *Proc. R. Soc. London, Ser. A.* **1957**, *238*, 425. Bader, R. F. W. *Can. J. Chem.* **1962**, *40*, 1164.

(24) Burdett, J. K. "Molecular Shapes"; Wiley: New York, 1980.

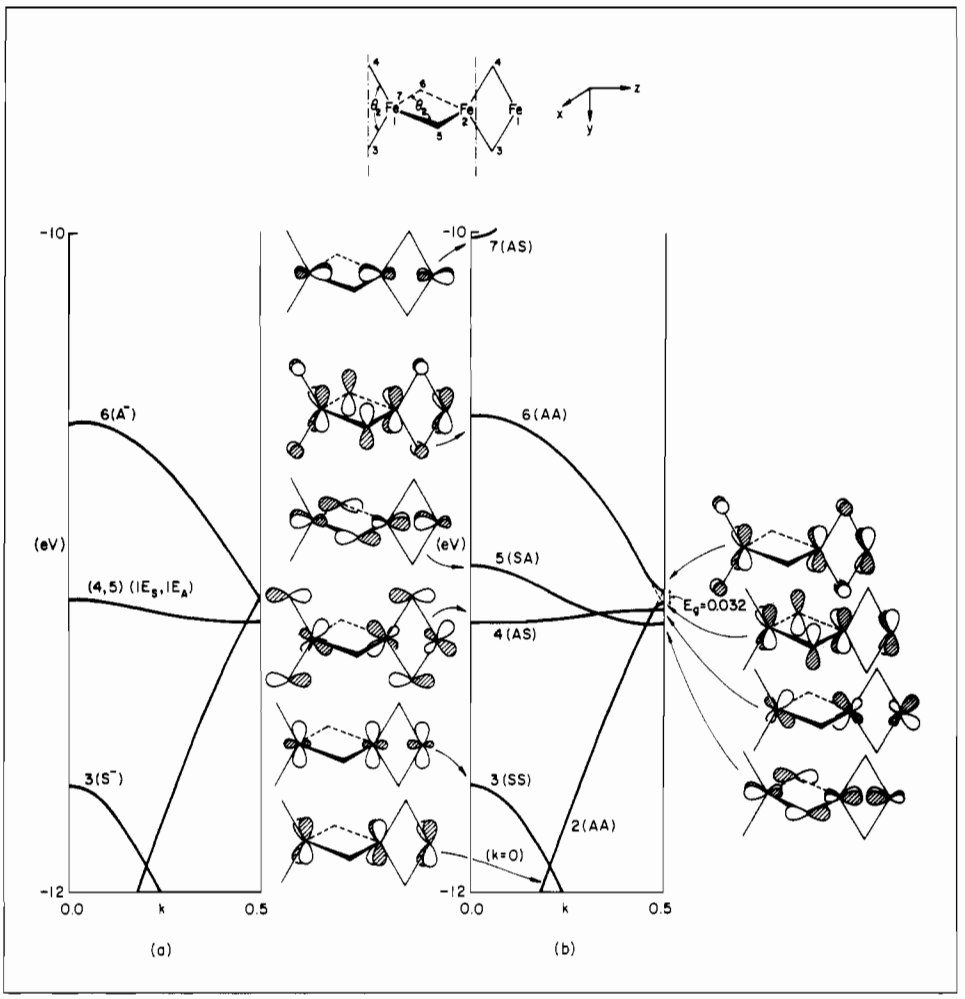

Figure 3. Band structure of the $(FeS_2)_\infty$ chain: (a) $\theta_2 - \theta_1 = 0°$; (b) $\theta_2 - \theta_1 = 3.0°$.

For a fixed M–S distance the amount of distortion may be monitored by the S–M–S angle θ, as indicated in **24**. An in-

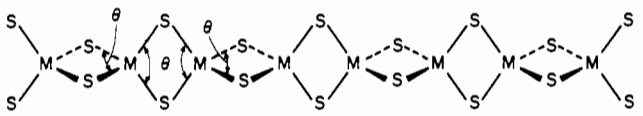

24

teresting example of an elongated chain is found in the recently reported[5] structure of $Na_5Co_2S_5$. The structure features $(CoS_2)_\infty$ edge-sharing tetrahedral chains running down the c axis of the tetragonal cell. The angle θ is relatively acute ($\sim$96.0°), giving rise to a long cobalt–cobalt distance (3.11 Å). A somewhat peculiar aspect of this material is the +2.5 oxidation state of the cobalt atoms. We will return to this point shortly.

For the time being the band structure of a $(CoS_2)_\infty$ chain with θ = 95.0° serves as a good starting point for our analysis of the electronic structure change associated with a variation of θ, and this is shown in Figure 4. Just as in Figure 2, and for the same reason ($\tilde{G}_k$ is isomorphic to C_{4v} along the line $k = 0 \rightarrow k = \pi/a$), the bands are labeled according to their symmetry property with respect to the xz plane (A or S) and the 4_2 screw axis (+ or −). Only those bands which are metal d centered are numbered, while those primarily on sulfur are unnumbered. The two pairs of metal d degenerate bands are labeled 1E and 2E. Note that there is no clear partitioning of the bands descending from the t_2 or e sets of the monomer tetrahedral crystal field. Obviously at this geometry local environment factors do *not* control the electronic structure of the system. The bands descending from the t_2 orbitals are again recognizable by metal–sulfur σ antibonding and are found in $2E$, $2S^+$, $1E$, and $1S^-$, sweeping down the energy scale. Bands $1A^-$, $1S^+$, $1S^-$, and $1A^+$ originate from the e set.

That the overall electronic structure of the system is dictated by interunit cell interactions rather than direct metal–metal overlap is indicated by several features. First the upper degenerate band is metal–metal bonding at $k = 0$ and lies much higher than the 1E band, which is metal–metal antibonding in character. Also the $2S^-$ band starts low in energy due to a favorable metal–sulfur-bonding interaction and in spite of the strong σ antibonding between adjacent metal atoms. This band would actually be lower in energy at $k = 0$, but it undergoes an avoided crossing with $1S^-$ as witnessed by the interchange of metal d character in these two bands at the zone center. If we look now at the slope of the bands, 2E drops in energy as one goes away from $k = 0$. If metal–metal interactions were dominant, this band would behave in the opposite way. Along the line, more and more antibonding is introduced between metal atoms, but this is overridden by an increase in metal–sulfur bonding. The slope of 1E is somewhat unexpected (it should be negative whether M–M or M–S interactions dominate) until one realizes that 1E undergoes a strong avoided crossing with the lower sulfur-centered E band.

Before we open the angle θ, we note that $Na_5Co_2S_5$ would be metallic in a low-spin configuration. The corresponding Fermi level is indicated by $\epsilon_F(d^{6.5})$ in Figure 4. However, we anticipate the life is not so simple and the system is likely to choose an electronic configuration where bands 1E, $2S^-$, $1A^-$, and $2S^+$ are occupied partially with paired spins and partially with unpaired spins. It should be noted that the topology of the bands could allow the coexistence of magnetism and electrical conductivity. We encourage further physical measurement on this system. Finally it is interesting to notice that a diamagnetic d^8 system would be a semiconductor with an indirect gap of $\sim$0.21 eV between the top of $2S^+$ and the bottom of 2E. One way to achieve this electron count would be to make $Ca_3Na_2Co_2S_5$, substituting 60% of the sodium atoms by calciums. The ionic radii of Na^+

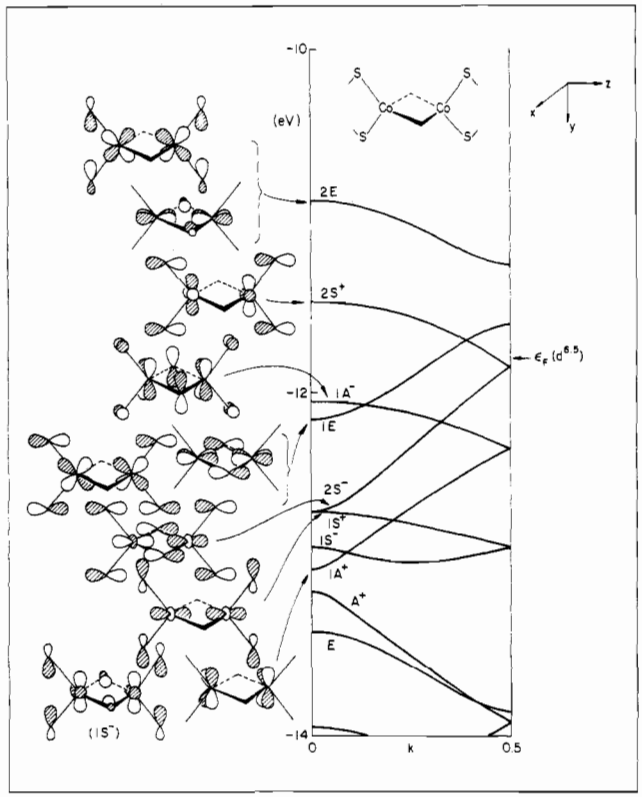

Figure 4. Band structure of the $(CoS_2)_\infty$ chain at $\theta = 95.0°$.

and Ca^{2+} are roughly similar (0.95 and 0.99 Å respectively), and cation-substitution experiments on $Na_5Co_2S_5$ may lead to the desired product.

If we return to the band structure of the $(CoS_2)_\infty$ chain, what happens if θ in **24** is allowed to relax towards greater values? Figure 5 shows the band structure of the chain for $\theta = 95.0$, 102.5, 110.0, and 117.5°. The solid lines are bands descending from the t_2 set of the tetrahedral pattern, metal–sulfur antibonding. The dashed lines represent those bands originating from the e set. Finally the thin solid lines stand for sulfur-centered bands.

There is clearly a gradual modification of the band structure when the chain is contracted. In dealing with discrete molecules, one can usually understand the electronic changes associated with a given geometrical perturbation by plotting the MO energies against the variations in the parameter that monitors the deformation, the familiar Walsh diagram. When one deals with a solid, three and not one factors are important and contain the information we seek: the center of gravity of the band, the sign of its slope, and the bandwidth. In the following we discuss in some detail the interplay between these three factors in connection with the picture of Figure 5.

As a starting point let us consider only the metal–sulfur interactions. It is clear that both the mean band energy and the band widths are determined by these. The idea is that a strong metal–sulfur interaction within the unit cell is also a strong metal–sulfur interaction between unit cells, which in turn governs the band dispersion. All this is basically set by the crystal field splitting. For this reason we first show in Figure 6 the variation of the metal d orbitals as a function of θ in a tetrahedral CoS_4 unit. For future reference we appended to the d character of the orbital the labels of the corresponding bands when the solid is formed; see Figure 4. Because it is not important in the context of the present discussion, the hybridization in d_{yz} and d_{xz} is omitted in Figure 6. Starting with $\theta = 109.47°$, let us comment briefly on Figure 6. At the perfect tetrahedral angle the upper three orbitals are degenerate, as prescribed by group theory.[25] When θ decreases, the point group symmetry is lowered from T_d to D_{2d}: the t_2 set splits into an e set (d_{yz},d_{xz}) and a b_2 orbital. The e set goes up in energy due to more metal–ligand σ antibonding, as shown in **25** → **26** for d_{yz}, and b_2 drops for the opposite reason.

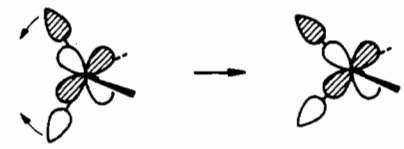

25 **26**

Also the initial degeneracy between d_{z^2} and d_{xy} is lifted. At $\theta = 109.47$ these orbitals are σ nonbonding,[26] and very little interaction is turned on upon distortion. The degeneracy is split (into a_1 and b_1), but both orbitals remain approximately constant in energy.

Parenthetically we should notice that a plot of the total energy for a high-spin d^7 system features a minimum at $\theta \simeq 110.0°$, in nice agreement with the recently reported[27] structure of Na_6CoS_4. This gives us some confidence in the magnitude of the bandwidths of Figure 5.

From Figure 6 it would be reasoned that an increase in θ should lower the center of gravity of 1E and 2E bands. Also the bands should be less dispersed. As seen in Figure 5, this is exactly what happens. Note that the slope of 2E is eventually reversed at $\theta = 117.5°$. We will return to this when the influence of the metal–metal interaction is dealt with. With a focus now on the ($2S^+$,$2S^-$) pair of bands, that is $d_{x^2-y^2}$ in Figure 6, the bands should be shifted up in energy upon increase of θ. They are. However the increase in metal–sulfur interaction should translate into a larger band width. The opposite occurs in Figure 5. A careful look at the right-hand-side plot of Figure 5 shows that $2S^-$ is actually prevented from going deeper in energy at $k = 0$ by the strong avoided crossing it undergoes with $1S^-$. The behavior of d_{xy} in Figure 6 tells us that the ($1A^+$,$1A^-$) pair of bands should remain unaltered in terms of their widths and position on the energy scale as a function of θ. This turns out to be true except for the bottom of band $1A^+$, slightly pushed up by sulfur-centered A^+ in the distortion. Finally, the bands originating from d_{z^2} ($1S^+$,$1S^-$) should be unchanged upon variation of θ. A look back at Figure 5 clearly establishes that this expectation is not met. Both the slope and the bandwidth of the ($1S^+$,$1S^-$) pair are dramatically modified upon increasing θ.

So far we have discussed the pattern of Figure 5 in terms of the metal–sulfur–metal interactions of whay we may call through-bond coupling. We now include the effect of the metal–metal interactions, or the through-space coupling. Returning to band 2E, we noted that a change in the sign of the slope of this band has occurred from $\theta = 95.0°$ to $\theta = 117.5°$. This simply means that the inter unit cell interactions are not governed by metal–sulfur interactions at large values of θ but rather by those between metal atoms. Recall that along the symmetry line more and more nodes are inserted in the crystal orbital between adjacent unit cells. For a small value of θ the metal–sulfur antibonding dominates the overall character of the crystal orbital. Increasing k diminishes these unfavorable interactions, and 2E has a negative slope. At a large value of θ, the net behavior of the crystal orbital is dictated by the metal–metal interactions. Those are bonding at the zone center and become more and more antibonding. This is illustrated in **27** where only the d orbital is drawn out along

27

(25) Cotton, F. A. "Chemical Applications of Group Theory", 2nd ed.; Wiley: New York, 1971.

(26) These are also π antibonding with respect to the other pair of ligands. This interaction is relatively constant within the range of values of θ discussed here.

(27) Klepp, K.; Bronger, W. *Z. Naturforsch., B: Anorg. Chem. Org. Chem.* **1983**, *38B*, 12.

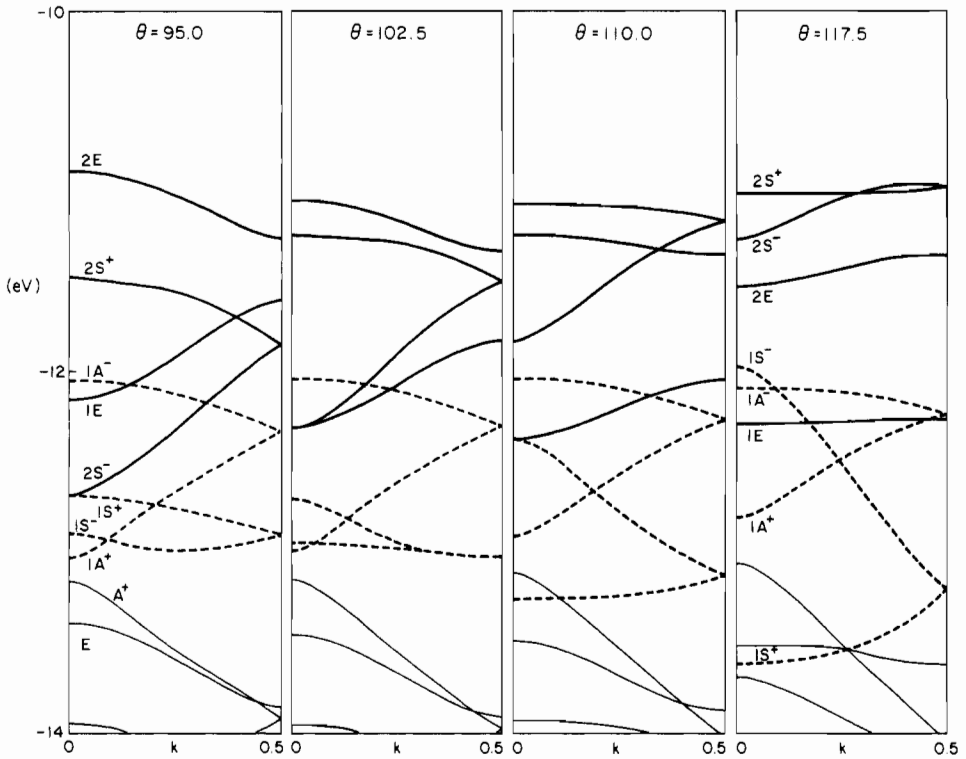

Figure 5. Band structure of the $(CoS_2)_\infty$ chain at different angles θ. From left to right the chain is contracted.

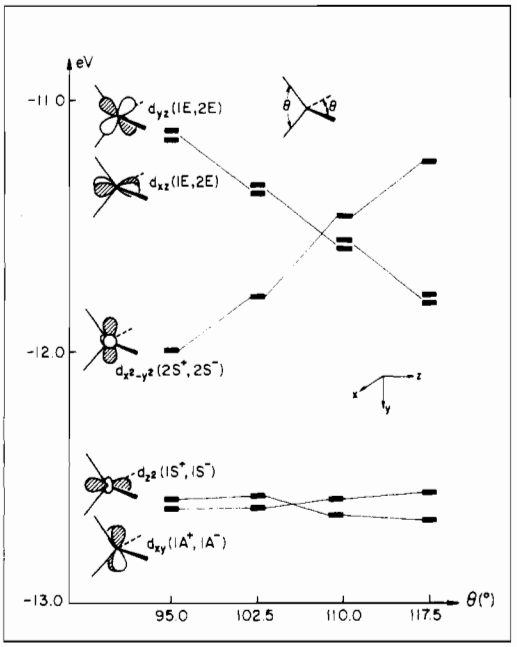

Figure 6. Walsh diagram for the distortion away from tetrahedral symmetry of a MS_4 unit.

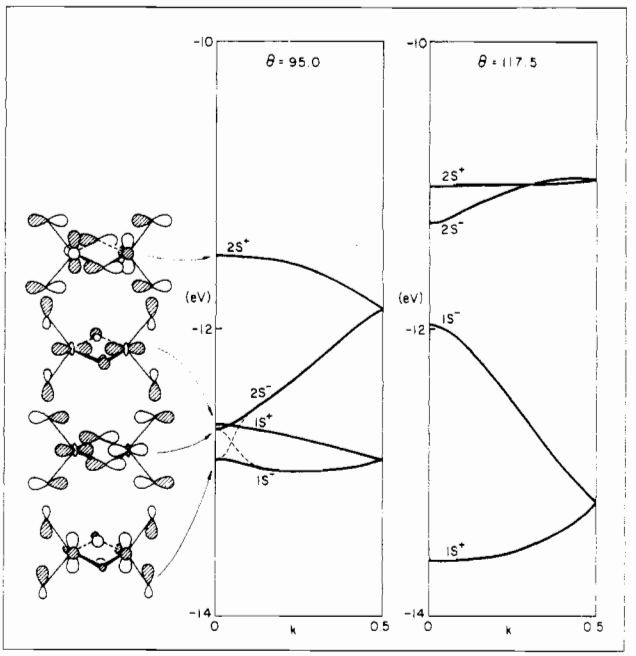

Figure 7. Bands 2S and 1S of the $(CoS_2)_\infty$ chain at $\theta = 95.0°$ (left) and $\theta = 117.5°$ (right).

the chain. Similar reasoning may be applied to understand the flattening of the 1E band upon increase of θ. The only difference is that this band is both metal–sulfur and metal–metal antibonding at the zone center. Bringing the metal atoms closer to each other (by opening θ) reinforces the influence of the metal–metal interactions in terms of the overall behavior of the band. These interactions, increasing in numbers as k increases, stabilize more and more the crystal orbitals and tend to cancel the effect of the unfavorable metal–sulfur interactions.

The most drastic changes in the band structure of the chain as θ varies are found in the $1S^+$, $1S^-$, $2S^+$, and $2S^-$ bands. The crystal field effects, as discussed above, do not account for all these modifications, and one has the feeling that through-space interactions are of major importance here. The best way to visualize this is to focus on what is happening between these four bands at $\theta = 95.0°$ and $\theta = 117.5°$. The situation in each case is depicted schematically in Figure 7, where we have indicated the previously noted avoided crossing between $1S^-$ and $2S^-$ with a dashed line. Note first that the 2S band as a whole is characterized by metal–metal δ overlap and metal–sulfur σ overlap. Conversely, the 1S band contains interactions controlled by metal–metal σ and metal–sulfur π types of overlap. At $\theta = 95.0°$ the energy of the top of band $2S^+$ is governed by extremely strong metal–sulfur interactions; see left-hand side of Figure 7. As k increases the phase relationship between some pairs of metal atoms (those belonging to adjacent cells), is reversed, so that the d orbitals become actually inphase with each other. This has the crucial consequences of allowing a different sulfur orbital to mix in. For

a given pair of metal atoms along the chain, the interaction goes from **28** to **29**. It is clear that less antibonding is present in the

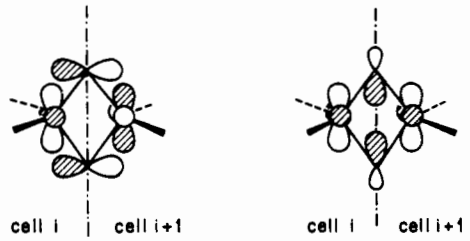

28 **29**

latter than the former. At the zone boundary, $2S^+$ folds back and the phase changes between d orbitals occur now in pairs of atoms of the same unit cell. The process described in **28** and **29** takes place in the xz plane as shown in **30** and **31**. Eventually at the

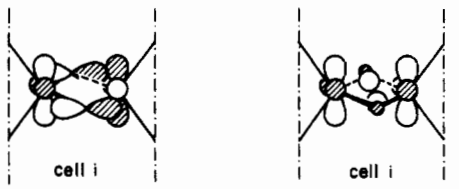

30 **31**

bottom of $1S^-$ all the interactions are of type **29** and **31**. The tremendous decrease of the metal–sulfur σ antibonding in the whole $x^2 - y^2$ band ($2S^+$,$2S^-$) lies at the heart of the large dispersion in the band structure. What could prevent $2S^-$ from going that deep in energy? Obviously $1S^-$ is the answer. However the most metal–metal σ antibonding, found for $1S^-$ at $k = 0$, is not enough at this value of θ.

If we turn our attention to the picture at $\theta = 117.5°$ in Figure 5, it is clear that now the antibonding between the z^2 orbital of the metal is strong enough to push up the bottom of $2S^-$. The large dispersion is governed by through-space interaction in this case.

What is the overall picture? At any angle, metal–sulfur-antibonding bands, descending from the t_2 set of the tetrahedral pattern, mix into those of the e set. Never does one find a gap between t_2 and e bands like the one existing between t_{2g} and e_g bands in face-sharing octahedral systems.[22c] The reason is that the crystal field splitting of an octahedral complex is much larger than that of a tetrahedral one.[28] In the tetrahedral chain the band dispersion is large enough to disturb the ordering of the levels set by crystal field effects. Contraction or elongation of the chain, however, dictates which "t_2" bands undergo mixing and to what extent they do so. For example, at small θ, metal–metal interactions become important. It is those metal–sulfur-antibonding states that are metal–metal bonding (1E) which are "drowned" in the "e" bands.

It is interesting to notice that a substantial band gap is opened between $1S^-$ and 2E upon contraction of the chain. As noted earlier for $(FeS_2)_\infty$ there may be a change of obtaining a d^6 material with semiconducting behavior. One could worry about filling a strong metal–metal antibonding band, the top of $1S^-$, and the instability associated with this process. However, the avoided crossing between $2S^-$ and $1S^-$ assures that the strongest z^2/z^2 antibonding of $1S^-$ is in actual fact transferred to the bottom of $2S^-$. As indicated in Figure 7 (right), if anything the top of $1S^-$ is metal–metal δ bonding. We believe that reduction of $Na_5Co_2S_5$ by half an electron and compression of the material along the c axis may yield diamagnetic semiconductor systems.

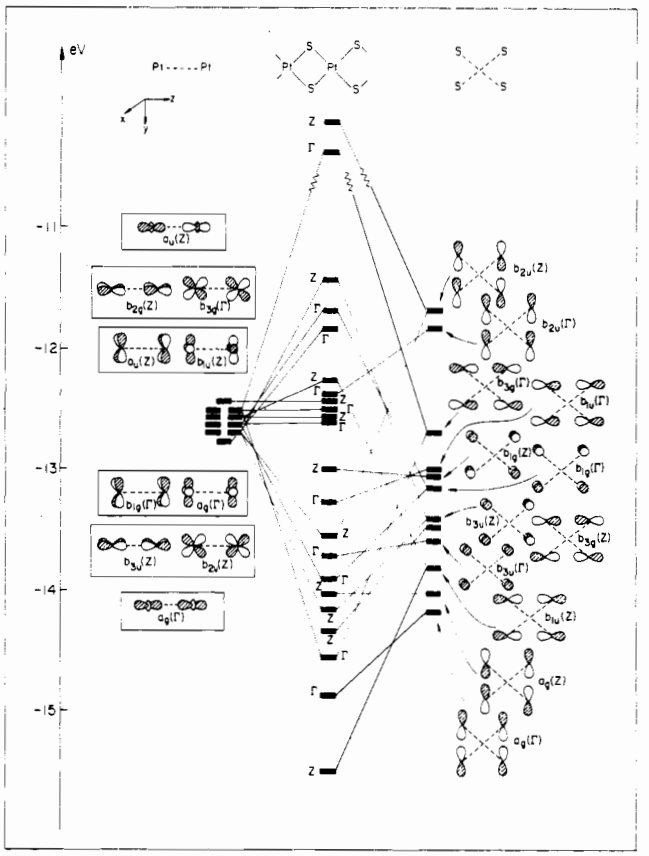

Figure 8. A fragment within the solid construction of the $(PtS_2)_\infty$ band structure.

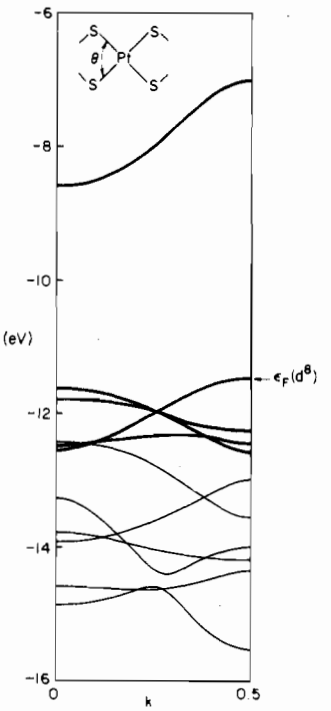

Figure 9. Band structure of the $(PtS_2)_\infty$ chain at $\theta = 80.0°$.

The Square-Planar System

Edge-sharing square-planar chains of type **4** are mostly encountered in systems with stoichiometry A_2MX_2, where A is an alkali metal, M is Pt or Pd, and X is a main-group element. When X belongs to group 15,[37] an X–X bond exists[29] and the chain is

(28) Huheey, J. "Inorganic Chemistry", 3rd ed.; Harper and Row: New York, 1983.

(29) Schuster, H.-U.; Rősza, S. *Z. Naturforsch., B: Anorg. Chem. Org. Chem.* **1979**, *34B*, 1167. Rősza, S.; Schuster, H.-U. *Ibid.* **1981**, *36B*, 1666.

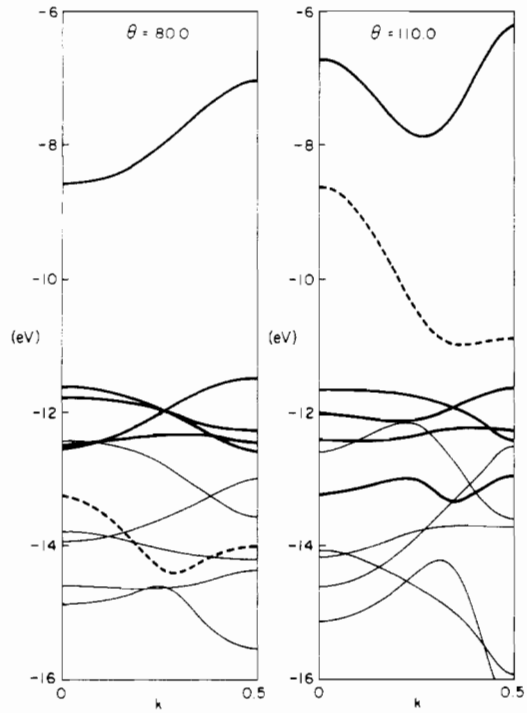

Figure 10. Band structure of the $(PtS_2)_\infty$ chain at $\theta = 80.0°$ (left) and $\theta = 110.0°$ (right).

actually puckered. The electronic factors governing this distortion have been analyzed elsewhere.[30] We should perhaps mention here the existence of a number of Pt dimer complexes which feature bridging sulfide of alkyl sulfide ligands and which display a local square-planar environment around the metal atoms.[31] In this closing section we would like to focus on the $(PtS_2^{2-})_\infty$ system and briefly analyze the influence of the metal–metal distance on the electronic structure and physical properties of this material.

The band structure of $(PtS_2^{2-})_\infty$ may be constructed using a variety of ways. In what follows we adopt the "fragment within the solid" approach developed by Burdett.[32] The idea is to partition the extended solid into two sublattices and interact the crystal orbitals of each at $k = 0$ and $k = \pi/a$.

In the case under consideration we use an infinite chain of metals for the first fragment and the frame defined by the sulfur atoms for the second. Figure 8 shows how the crystal orbitals at the zone center and zone boundary are obtained. The orbitals of the two fragments are classified according to D_{2h}, since this is the point group of $\vec{k}$ at Γ (the zone center) and Z (the edge). Also appended is a symbol that indicates the translational symmetry of the fragment orbitals, Γ or Z. The combination of the fragment orbitals is carried out by following the usual rules; i.e., orbitals of the same symmetry (point group *and* translation) interact to produce bonding and antibonding states. The d orbitals of the Pt chain are not split due to the long Pt–Pt distance, 3.55 Å. Interestingly, all the sulfur combinations are pushed down in energy except two that are destabilized by the Pt orbitals ($b_{2u}(Z)$ and $b_{2u}(\Gamma)$). The reason is that they start higher in energy than the d block of the Pt chain. In turn this is the result of σ antibonding between sulfur atoms along the relatively short sulfur–sulfur distance, 3.11 Å. The geometry used for the calculation is that found experimentally with θ (see **4**) = 80.0°. A qualitative band structure may be constructed from the information provided by the middle of Figure 8. We have there the two end points (Γ and Z) for each band. In connecting these points, one must take into account that the point group of $\vec{k}$ is C_{2v} along the line and therefore we must watch for avoided crossings. Figure 9 shows the results of a full calculation. The information of Figure 8 serves to identify the topology of the crystal orbitals at the end points of the zone. The thick solid lines are metal-d-centered bands and the thin solid lines are sulfur-centered bands. The Fermi level for the d^8 electron count, that of the $Na_2Pd(Pt)S_2$, K_2PtS_2, and Rb_2PtS_2 systems, is indicated with an arrow at ϵ_F. Clearly these materials are insulators, with a sizable band gap of ~3.5 eV. The picture coming out of Figure 9 is a four-band below one-band pattern for the metal-d-centered orbitals with only the lowest four being filled. The upper band is metal–sulfur σ antibonding, and the band structure is a nice reflection of the square-planar crystal field splitting[28] around the platinum atom.

The immediate idea that comes to mind in order to make this series of chains more attractive in terms of their electrical properties is doping. In particular, partial filling of the conduction band could induce metallic behavior in this system. Given the tunnel-like structure of all the d^8 materials synthesized so far, we think that partial substitution of alkaline-earth-metal atoms for the alkali-metal atoms may be a feasible process.

How does contraction of the chain alter the pattern of Figure 9? Figure 10 provides the answer. At left is the band structure of the $(PtS_2)_\infty$ chain at $\theta = 80.0°$, at right that for $\theta = 110.0°$. Again thick (thin) solid lines stand for metal-d- (sulfur-) centered radicals. The dashed line indicates the band that is boosted up in the distortion. At $k = 0$ the corresponding crystal orbital appears as shown in **32**. It is sulfur centered and pushed up in

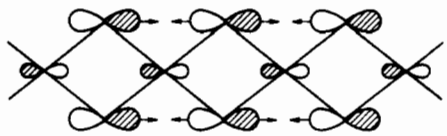

32

energy by sulfur–sulfur antibonding (see arrows). There is also some metal p mixed in **32**, but our computations indicate that the band is most heavily concentrated on the sulfur atoms. The calculations show that for all electron counts $d^6 - d^9$, the compression of the chain is energetically unfavorable due to overwhelming sulfur–sulfur lone-pair repulsion. Interestingly, at all angles (θ = 80, 90, 100, 110°) the Pt–Pt overlap population is negative for a d^8 system. This imply results from the fact that the top of each metal d band is more destabilized than the bottom is stabilized upon distortion. This follows the familiar four-electron two-orbital destabilizing interaction in a discrete system and further confirms that the electronic structure of edge-sharing square planes is governed by crystal field effects and on-site symmetry.

Conclusions

In this contribution we have tried to take a step further toward an understanding of the bonding in solids, especially those in which there is a potential role for main-group bridging atoms and metal–metal interactions. The electronic structure of discrete transition-metal complexes is primarily governed by crystal field or ligand field effects. In an extended structure, the bonding and physical properties are controlled by a combination of crystal field (local) factors and longer range interactions affecting the band dispersion. It appears that the patterns determined by the metal local environment only may be modified more or less seriously by effects arising from translational periodicity—inter unit cell interactions. This is what we saw and analyzed in detail for the edge-sharing tetrahedral chain. One consequence is the occasional removal of a clear-cut separation between "favorable" and "unfavorable" electron counts, where such electron counts might have been imagined to be set by the local metal coordination environment. The flexibility so attained can lead to the design

(30) Underwood, D. J.; Novak, M.; Hoffmann, R. *J. Am. Chem. Soc.* **1984**, *106*, 2837.
(31) (a) Briant, C. E.; Gardner, C. Jj.; Andy Hor, T. S.; Howells, N.; Mingos, D. M. P. *J. Chem. Soc. A* **1970**, 1243. Briant, C. E.; Andy Hor, T. S.; Howells, N. D.; Mingos, D. M. P. *J. Chem. Soc., Chem. Commun.* **1983**, 1118. (b) Ugo, R.; LaMonica, G.; Cenini, S.; Segre, A.; Conti, F. *J. Chem. Soc. A* **1971**, 522.
(32) Burdett, J. K. *J. Am. Chem. Soc.* **1980**, *102*, 5458.

Table II. Parameters Used in the Calculations

orbital		H_{ii}, eV	ζ_1	ζ_2	C_1[a]	C_2[a]
Co	3d	−13.18	5.55	2.10	0.5679	0.6059
	4s	−9.21	2.00			
	4p	−5.29	2.00			
S	3s	−20.00	1.817			
	3p	−13.3	1.817			
Fe	3d	−12.70	5.35	1.80	0.5366	0.6678
	4s	−9.17	1.90			
	4p	−5.37	1.90			
Pt	5d	−12.59	6.013	2.693	0.6334	0.5513
	6s	−9.08	2.554			
	6p	−5.48	2.554			

[a] These are the coefficients in the double-ζ expansion.

of novel conducting systems.

Acknowledgment. We thank M.-H. Whangbo and our research group for useful discussions and W. Bronger for communicating his results to us prior to publication. Our research was supported by the National Science Foundation through research Grant CHE 8406119 and research Grant DMR 8217227 A02 to the Materials Science Center at Center at Cornell University. Many thanks are due to Ellie Stagg for the typing and Jane Jorgensen and Elisabeth Fields for the drawings.

Appendix

The Fe–S, Co–S, and Pt–S distances were set at 2.25, 2.317, and 2.36 Å, respectively. The values of the S–M–S angles for each calculation are given in the main body of the text.

The computations were carried out by using a tight-binding scheme implemented[33] in the extended Hückel framework.[34] The H_{ii}'s are listed in Table II and were taken from previous work.[35,36] The band structures were obtained by solving the eigenvalue equation at five points of the Brillouin Zone: $k = 0.0, 0.125, 0.250, 0.325, 0.500$. When an average quantity was computed (energy, overlap population) a mesh of 20 k-points was used.

Note Added in Proof. Recently Bronger and co-workers have proposed[38] an explanation for the low-spin state of d^5 and d^6 $(FeS_2)_\infty$ chains. Their model is based on crystal-field splitting considerations and goes as follows: An iron atom is surrounded by four sulfur atoms to generate the usual two-below-three pattern. Furthermore, two positive irons are attached along the propagation axis. That provides an attractive term which stabilizes z^2 most (the three Fe atoms lie along the z axis), xz and yz next. The level splitting so obtained is shown in **33a**.

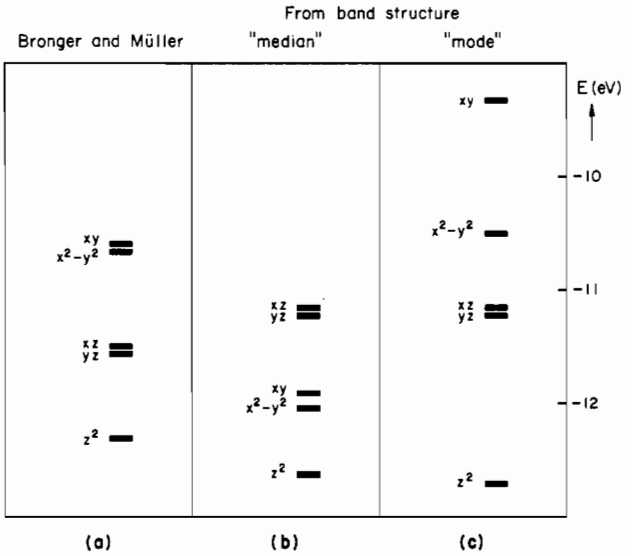

33

We tried to correlate this plausible model with our results, but given the delocalized nature of the bands, we run into the problem of defining an orbital energy from a band structure. We explored two choices affording the effective splitting patterns shown in **33b** and **33c**. In the former, the contributions of the various d orbitals were projected out of the total DOS resulting from Figure 2. Then the 50% filling mark for each orbital—the median—was picked as the effective orbital energy. The two models agree on both the position of z^2 (lowest) and on the predicted low-spin nature of a d^5, d^6 system. However, xz and yz are inverted with respect to xy and $x^2 - y^2$.[39,40] In **33c**, we selected instead the energy of highest density of states—the mode—for the orbital under consideration. The picture agrees somewhat better with that of **33a**. Interestingly, the three viewpoints agree in their qualitative conclusions. Yet, given the substantial band dispersions displayed in Figure 2, we are inclined to believe that the delocalized picture provided by the band structure in the final analysis affords a better understanding of the situation.

Registry No. FeS_2, 12068-85-8.

(33) Whangbo, M.-H.; Hoffmann, R.; Woodward, R. B. *Proc. R. Soc. London, Ser. A* **1979**, *366*, 23.
(34) Hoffmann, R. *J. Chem. Phys.* **1963**, *39*, 1397. Hoffmann, R.; Lipscomb, W. N. *Ibid.* **1962**, *36*, 2179.
(35) Hoffman, D. M.; Hoffmann, R. *J. Am. Chem. Soc.* **1982**, *104*, 3858.
(36) Wijeyesekera, S. D.; Hoffmann, R. *Inorg. Chem.* **1983**, *22*, 3287.
(37) In this paper the periodic group notation is in accord with recent actions by IUPAC and ACS nomenclature committees. A and B notation is eliminated because of wise confusion. Groups IA and IIA become groups 1 and 2. The d-transition elements comprise groups 3 through 12, and the p-block elements comprise groups 13 through 18. (Note that the former Roman number designation is preserved in the last digit of the new numbering: e.g., III → 3 and 13.)
(38) Bronger, W.; Müller, P. *J. Less-Common Met.* **1984**, *100*, 241. Bronger, W. *Pure Appl. Chem.*, in press.
(39) Note the energy scale for **33b,c** is not the same as for **33a**. The latter is parametric.
(40) A speculative explanation for this discrepancy involves "orbital character transfer" via avoided crossings.